optica

Ultrafast optical switching and power limiting in intersubband polaritonic metasurfaces

Sander A. Mann,[1,†,*] Nishant Nookala,[2,†] Samuel C. Johnson,[3] Michele Cotrufo,[1] Ahmed Mekawy,[1,4] John F. Klem,[5] Igal Brener,[5] Markus B. Raschke,[3] Andrea Alù,[1,2,4,6] and Mikhail A. Belkin[2,7]

[1]Photonics Initiative, Advanced Science Research Center, City University of New York, New York, New York 10031, USA
[2]Department of Electrical and Computer Engineering, The University of Texas at Austin, Austin, Texas 78712, USA
[3]Department of Physics, Department of Chemistry, and JILA, University of Colorado at Boulder, Boulder, Colorado 80309, USA
[4]Department of Electrical Engineering, City College of The City University of New York, New York, New York 10031, USA
[5]Sandia National Laboratories, Albuquerque, New Mexico 87185, USA
[6]Physics Program, Graduate Center, City University of New York, New York, New York 10016, USA
[7]Walter Schottky Institute, Technical University of Munich, Garching 85748, Germany
*Corresponding author: smann@gc.cuny.edu

Received 30 November 2020; revised 14 March 2021; accepted 15 March 2021 (Doc. ID 415581); published 29 April 2021

Highly nonlinear optical materials with fast third-order nonlinear optical response are crucial for the operation of all-optical photonic devices, such as switches for signal processing and computation, power limiters, and saturable absorbers. The nonlinear response of traditional optical materials is weak, thus requiring large light intensities to induce significant changes in their properties. Here we show that optical control of the coupling rate in subwavelength patch antennas coupled to intersubband transitions in multi-quantum-well semiconductor heterostructures can provide a giant third-order nonlinear response, on the order of $3.4 \times 10^{-13} m^2/V^2$, with a response time <2 ps. We utilize this effect to realize intersubband polaritonic metasurfaces and demonstrate their operation as highly nonlinear saturable and reverse saturable absorbers, enabling optical power limiters and other elements for all-optical modulation and control. Our approach enables a plethora of compact, low-power, highly nonlinear devices with spectral, temporal, and structured wavefront responses tailored by design.

https://doi.org/10.1364/OPTICA.415581

1. INTRODUCTION

Highly nonlinear metasurfaces are desirable for a wide range of applications, including wave mixing without phase-matching constraints, all-optical switching and beam steering, optical limiting, and phase conjugation. With these functionalities in mind, a number of approaches have been pursued to achieve large $\chi^{(2)}$ and $\chi^{(3)}$ in metasurfaces [1], using intrinsic metal [2,3] or dielectric [4–7] nonlinearities, epsilon-near-zero materials [8–13], and coupling to J-aggregates or other molecules [14–18]. It has recently been shown that intersubband polaritonic metasurfaces, based on coupling between subwavelength patch antenna resonators and intersubband transitions in multi-quantum wells (MQWs), can produce an effective $\chi^{(2)}$ far exceeding other approaches [19,20]. Their unique nonlinear response stems from the combination of quantum engineering of the electronic states in the MQW heterostructure, which by itself enables one of the largest known nonlinear responses in bulk materials [21–24], with photonic engineering of the resonance field profiles. These engineered resonances support highly confined, strong electric fields ideally overlapped with the MQW transition dipole moment driving the nonlinearity. Using this approach, metasurfaces with a tailored nonlinear response have recently been demonstrated [25–28] across a wide range of frequencies, from the near to far infrared.

The nonlinear conversion efficiency of intersubband polaritonic metasurfaces is ultimately limited by intensity saturation [29]. Here, we show that this mechanism, driven by depletion of the ground state of the MQW, can be used to our advantage to demonstrate extreme third-order nonlinearity beyond the limits of perturbative responses [Figs. 1(a) and 1(b)]. Depletion of the ground state reduces the intersubband oscillator strength, which in turn reduces the effective coupling rate between the antenna resonance and the intersubband transition [30,31]:

$$\Omega_{\text{eff}}^2 = \Omega_R^2 (n_g - n_e), \tag{1}$$

where n_g and n_e are the ground and excited state occupancies in the MQW (assuming that it can be described by a two-level system), respectively, and Ω_R is the vacuum Rabi frequency [the splitting between peaks at low intensity is approximately $2\Omega_R$, see Fig. 1(c)].

Nonlinear tunability of the coupling coefficient enables control over the system response: in the unsaturated case coherent energy transfer occurs between the antenna resonance and the intersubband transition [15,32], while in the saturated case only

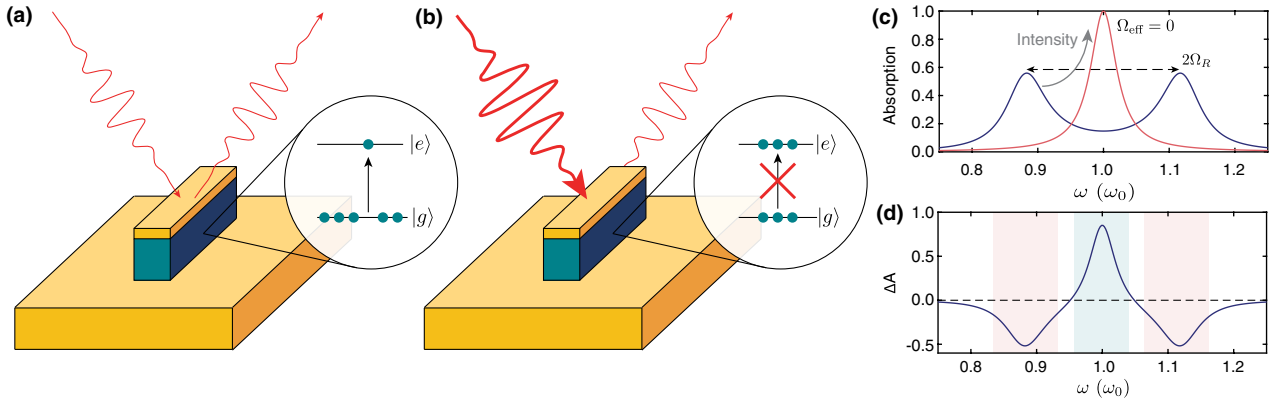

Fig. 1. Ultrafast, highly nonlinear metasurface with saturable and reverse saturable absorption and optical power-limiting functionalities. (a) At low intensities, a nanoantenna is strongly coupled to an intersubband transition in the underlying MQW substrate (shown in blue-green). As a result, polariton splitting is observed at the central frequency and the incident radiation is fully reflected. (b) At high intensities, the intersubband transition is saturated, and the antenna resonance is not strongly coupled to it. The incident pulse is now largely absorbed, leading to a limiting response. (c) The simulated low-intensity spectrum shows a clear signature of mode splitting due to strong coupling, while at high intensity, only the antenna resonance is observed due to saturation of the intersubband transition (see Eq. 1). (d) Change in metasurface absorption between low- and high-intensity illumination, highlighting saturable absorption (pink shading) and reverse-saturable absorption (green shading).

the resonator is effectively excited. In the frequency domain, this implies a transition from two resonant peaks in the unsaturated regime, due to polaritonic splitting, to a single peak in the spectrum when the transition is saturated [Figs. 1(c) and 1(d)]. This nonlinear transition from strong to weak coupling has been observed in, for example, semiconductor microcavities [31,33], plasmonic arrays coupled to molecules [14,15,18], and defect modes in metal/multi-quantum well photonic crystals [30,34]. Here, we demonstrate the nonlinear transition from strong to weak coupling in a polaritonic metasurface, where the constituent building blocks, or meta-atoms, are subwavelength metal patch antennas coupled to a multi-quantum well [see Fig. 1(a)]. The nonlinear optical response of these metasurfaces is principally determined by the local response of the meta-atom, which results in a largely angle-independent response (see Supplement 1), and it can be engaged without necessarily illuminating a very large area (i.e., with focused beams). Crucially, the approach demonstrated here opens up a pathway to structural and all-optical control of the wavefront of the reflected beam, analogous to previous demonstrations for metasurfaces [25,26].

To achieve strong spectral variations with intensity, as shown in Figs. 1(c) and 1(d), a large coupling rate with respect to the dephasing rates is required. In contrast, to achieve an ultrafast nonlinear response, the antenna and MQW linewidths have to be reasonably large. This implies that, for a strongly nonlinear response, the coupling constant has to approach the frequency of operation. This so-called ultrastrong coupling regime has recently been demonstrated in MQWs [35–38], with other systems rapidly following [39]. In this paper, we show that the synergy between MQW transitions and the antennas can dramatically enhance the coupling constant and nonlinear response, resulting in very low input powers required to trigger the transition at ultrafast speeds. The MQW transition is quantum engineered to have a large dipole moment and short upper state lifetimes (to achieve ultrafast speeds), while the antenna enhances the field in the MQW both through a large optical cross section and a moderate quality factor [40]. The resulting system is ideal to realize ultralow-power optical limiters based on reverse saturable absorption, which strongly reflect at low intensity but limit the amount of reflection at high intensity. At other frequencies, the system enables extremely sensitive saturable absorbers that work in reflection mode.

The paper is structured as follows: in the next two sections, we discuss the nonlinear optical properties of the polaritonic metasurface, followed by a demonstration of all-optical control in Section 4. Based on a theoretical model introduced and experimentally verified in Sections 2–4, we then evaluate the fundamental limits of resonant nonlinear optical limiters in Section 5, providing a pathway for further improvements to their performance. Finally, in Section 6, we numerically demonstrate all-optical nonlinear control of the wavefront of the reflected beam, highlighting the versatility of the platform.

2. POLARITONIC METASURFACES

An scanning electron microscope (SEM) image of the fabricated polaritonic metasurface is shown in Fig. 2(a). It is composed of an array of gold dipolar patch antennas [41–45], where the dielectric spacer layer between the gold substrate and a thin gold strip is an n-doped InGaAs/InAlAs MQW, as shown schematically in Figs. 1(a) and 1(b) (further details are provided in Supplement 1). The band diagram of a single period of the MQW layer is shown in Fig. 2(b). The MQW layer consisted of 26 period repetitions for a total thickness of approximately 400 nm. The transition frequency between the first and the second electron subbands in the MQW is $\nu_{21} \approx 40$ THz, as confirmed by absorption measurements (see Appendix A). The transition energy between the second and third subband is $\nu_{32} \approx 25$ THz, significantly detuned from ν_{21}.

To find good overlap between the antenna resonance and the intersubband transition, we vary the patch antenna length l_y, as shown in Fig. 2(c). The measured linear absorption spectra of the metasurfaces [in the absorption units of $A = (I_{\text{in}} - I_{\text{r}})/I_{\text{in}}$, where I_{in} is the incident and I_{r} is the reflected light intensity] shows a clear anticrossing when the patch resonance intersects the intersubband transition. The MQW transition dipole moment is out-of-plane, and hence, it cannot be excited by the normally incident radiation directly but couples very efficiently to the antenna [35,37,38,46]. The intersubband transition frequency, as expected from bulk absorption measurements, is shown by the white dashed line.

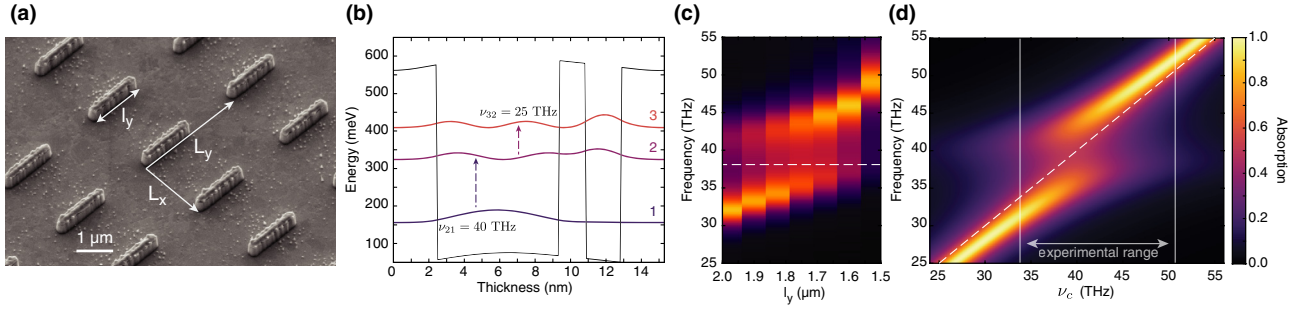

Fig. 2. Linear response of the polaritonic metasurface. (a) SEM image of the nonlinear metasurface under consideration, with the patch antenna size $l_x \approx 0.35$ μm and $l_y \approx 1.75$ μm and the unit cell size $L_x = 2.1$ μm and $L_y = 3.15$ μm, respectively. (b) Band structure of the asymmetric multi-quantum well, highlighting the 2–1 and 3–2 transition, which is purposefully detuned from the 2–1 transition. (c) Absorption spectrum measured with FTIR varying the antenna length l_y. A clear avoided crossing with the intersubband transition is observed. The dashed line indicates the transition frequency as obtained from bulk measurements. The color scale is shown in (d). (d) Absorption as calculated from Eq. (2) at low intensity, where the antenna frequency ν_c is varied rather than the antenna length. The range of measurements in (b) is highlighted.

We model the interaction between the metasurface and the multi-quantum well by combining coupled-mode theory with a Maxwell–Bloch model [47–50], where we approximate the MQW by N two-level quantum oscillators all coupled to the antenna with frequency g in the rotating wave approximation (see Supplement 1 for details):

$$\dot{a} = (i\omega_c - \gamma_r - \gamma_a - \gamma_s(w+1))\, a + iNgq + \sqrt{2\gamma_r} s_+$$

$$\dot{q} = (i\omega_c - \gamma_2)\, q - iga w$$

$$\dot{w} = 4g\Im\left(qa^*\right) - \gamma_1(w+1). \tag{2}$$

Here a is the complex plasmon amplitude [normalized so that $|a|^2$ is the stored number of photons], q tracks the evolution of the off-diagonal elements of the intersubband transition reduced density matrix [50], and $w = n_e - n_g$ is the inversion of the transition. The antenna and intersubband (ISB) transition have resonance angular frequencies ω_c and ω_q, and the MQW is further described by the total decoherence rate $\gamma_2 = 1/T_2$ and relaxation rate $\gamma_1 = 1/T_1$. Only the antennas are excited by the incident field amplitude s_+ (normalized so that $|s_+|^2$ is the number of incident photons per second). The antenna decays through radiation (γ_r) and absorption (γ_a), as well as through a saturation-related decay rate γ_s. This additional decay rate has to be included in the model, because the MQW cannot truly be described by a two-level system, but instead, there are transitions between higher excited states that become relevant at high intensity. In fact, at very high intensity, all electrons are promoted into the continuum, and the electromagnetic response becomes similar to that of a hot electron gas. The Rabi frequency is given by $\Omega_R = \sqrt{N}g$ (see Supplement 1).

The third-order nonlinearity in this model arises through the inversion w [see Eq. (2)], which affects the coupling between the two-level systems and the patch nanoantenna. Particularly, when the excited and ground state populations are equal, the quantum oscillators can no longer be coupled to, and the coupled system reduces to the patch antenna alone. In contrast, at low intensities, $w \approx -1$ and Eq. (2) simplifies to the well-known linear equations for coupled oscillators. We use the linearized equations to extract model parameters from the absorption measurements shown in Fig. 2(b) by fitting them simultaneously (see Supplement 1 for details). The linear response from the model is shown in Fig. 2(d), and it is in excellent agreement with the measurements shown in Fig. 2(c). In particular, for the metasurface with $l_y \approx 1.75$ μm shown in Fig. 2(a), we find $\omega_c = 251.1 \times 10^{12}$ rad/s, $\omega_q = 248.2 \times 10^{12}$ rad/s, $\gamma_r = 6.85$ THz, $\gamma_a = 1.34$ THz, $\gamma_2 = 27.6$ THz, and $\Omega_R = 31.8 \times 10^{12}$ rad/s. In the next section, we turn to the nonlinear response, and demonstrate multiple novel functional operating regimes for the nonlinear metasurface.

3. NONLINEAR INTENSITY DEPENDENCE

In Fig. 3(a), we show the metasurface absorption spectra at low (~70 kW/cm^2) and high peak intensity (~700 kW/cm^2), measured using a tunable ps laser (with an approximate 0.5 THz pulse bandwidth). At low peak intensity, we still observe the characteristic polaritonic splitting, but with reduced separation compared to the Fourier-transform infrared spectroscopy (FTIR) spectrum, while at higher peak intensity the polaritonic splitting vanishes, resulting in a single peak. This implies that the intersubband transition has been saturated sufficiently for it to be weakly coupled to the patch antenna. The experimental spectra are in good agreement with those predicted from the simple Maxwell–Bloch model, although the model only considers a single coupling strength to all N two-level systems.

Next, we consider the power dependence for three separate fixed frequencies, shown by the gray bands in Fig. 3(a). In Fig. 3(b) we consider the response at 35.5 THz, where there is a peak in absorption due to the lower polariton branch. As we increase the intensity, the mode splitting decreases, resulting in a reduction in absorption. In this regime, the metasurface acts as a saturable absorber. At 38 THz [Fig. 3(c)], we are slightly detuned from the lower polariton branch, and the absorption increases with intensity as the mode splitting reduces. Finally, at 40 THz [Fig. 3(d)], we observe a strong increase in absorption with increasing intensity. This frequency is close to the bare plasmon and intersubband transition frequencies and, as a result, it lies in between both low-intensity polariton branches. As the intensity is increased, the mode splitting vanishes, and we ultimately obtain a single peak with strong absorption. Interestingly, as the intersubband transition saturates, the absorption rates decrease, yet the overall absorption increases. This is because the system is engineered to be overdamped at low intensities, and with increasing intensity it approaches critical coupling [51], where the absorption and radiation loss rates are equal and at resonance the metasurface fully absorbs. At 40 THz,

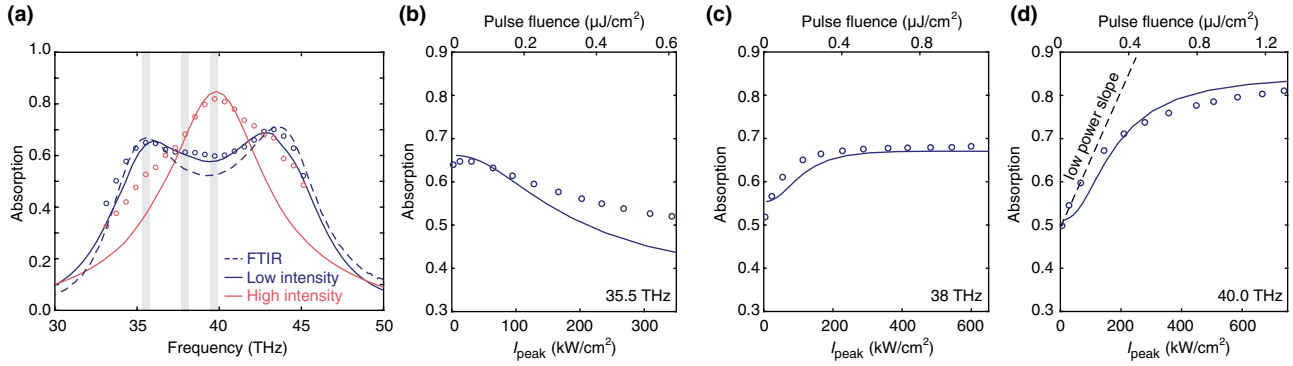

Fig. 3. Experimental nonlinear tuning of the coupling coefficient. (a) Absorption spectra at low (~70 kW/cm^2, blue) and high (~700 kW/cm^2, red) peak intensities, demonstrating the transition from strong to weak coupling of the polaritonic metasurface. We also show the FTIR absorption spectrum for comparison. (b) Absorption at 35.5 THz [left shaded region in panel (a)] as a function of peak intensity, demonstrating very large nonlinear absorption at low intensity. Experimental data are shown by circles, the predicted response from the model is shown with the solid line. (c) Same as in panel (b), but at 38 THz [middle shaded region in panel (a)]. In this case, we observe reversed saturable absorption (optical limiting) as the normal mode passes by. (d) Power dependence at 40 THz [right shaded region in panel (a)]. Here we observe maximal optical limiting for this sample. The black line shows the slope at low intensity, used to estimate the effective $\mathrm{Im}(\chi^{(3)}_{\mathrm{eff}})$.

we observe a change in absorption from 52% at low intensity up to 82% as the intensity increases.

To place the nonlinear response of the metasurface into context of other nonlinear materials, we estimate an effective nonlinear coefficient $\chi^{(3)}_{\mathrm{eff}}$ from the change in absorption at low intensities. To do so, we consider the metasurface (comprising subwavelength patch resonators and multi-quantum well) as a single homogeneous material with an effective nonlinear absorption coefficient $\beta_{\mathrm{eff}} = \Delta A/2d$, where ΔA is the change in the absorption due to illumination with intensity I after a double pass through the material with thickness $2d = 1$ μm. From Fig. 3(b), we find $\beta_{\mathrm{eff}} = 1.6 \times 10^7$ cm/GW, which can be converted into $\Im(\chi^{(3)}_{\mathrm{eff}}) = 3.4 \times 10^{-13}$ m^2/V^2 (see Supplement 1 for details). These values exceed naturally occurring ultrafast $\chi^{(3)}$'s by several orders of magnitude, and also appear stronger than photonic approaches to enhanced $\chi^{(3)}_{\mathrm{eff}}$'s based on plasmonics [1,3], ENZ [8,9], and two-dimensional [52,53] materials, or semiconductor saturable absorbers [54,55]. However, note that when comparing nonlinearity strengths across different frequency ranges, it must be considered that higher frequencies generally correspond to weaker material nonlinearities.

4. ALL-OPTICAL CONTROL

The change in absorption, both positive and negative, can be initiated by a separate pulse. To demonstrate this all-optical control in reflection, we show in Fig. 4 results from a degenerate pump-probe measurement. In these experiments, we excite the metasurface with a strong pump pulse at an angle of incidence around 30°. We simultaneously excite the metasurface under normal incidence with a weak probe pulse (<50 kW/cm^2) with variable delay. Depending on the center frequency, we obtain either an increase [Fig. 4(a), 35.5 THz] or a decrease in reflection [Fig. 4(b), 40 THz], as expected from the power dependence highlighted in Fig. 3. In both cases, we observe excellent agreement with the Maxwell–Bloch model (red solid line), where we have assumed that the pulse length is ~1.6 ps intensity full-width half-maximum (FWHM) and $T_1 = 1.7$ps, which is obtained from band structure calculations. Note that T_1 is dominated by nonradiative recombination, so that the optical environment has negligible effect on the decay rate. As evident from the pump-probe measurement, the metasurface response is ultrafast, despite the observed giant nonlinearity. The rise time of the system in our measurement is constrained by the pulse length, indicating that the system has nonlinear dynamics below the ps scale. The recovery time of the system is limited by the relaxation time of the excited state, $T_1 = 1.7$ ps, enabling ultrafast all-optical low-power manipulation of optical signals. It should be noted that, with a broadband probe pulse, richer dynamics such as the frequency shifts of the polariton branches or Rabi oscillations can be observed [15,32]. We are currently expanding our experimental capabilities to investigate these phenomena.

5. FUNDAMENTAL LIMITS TO OPTICAL LIMITERS

Having verified the accuracy of our Maxwell–Bloch model, we are able to investigate the fundamental limits to nonlinear light manipulation of our polaritonic metasurface in terms of reflection contrast. An ideal optical limiter fully absorbs when saturated, and at the same time, it fully reflects at low intensities. In our metasurface, Ohmic losses in the antenna (which are not affected by the input intensity) and in the saturated multi-quantum well fundamentally limit the lowest possible reflection that we can achieve. By requiring that at high intensity the saturated metasurface is perfectly absorbing, i.e., critically coupled, we find from our model that the absorption contrast $|\Delta A|$ between high and low intensity is given by

$$|\Delta A| = \frac{(1-f_s)^2}{\left(\frac{1+\eta}{1-\eta} + f_s\right)^2}, \tag{3}$$

where $\eta = \gamma_a/(\gamma_a + \Omega_R^2/\gamma_2)$ is the relative absorption loss in the optical resonator with respect to absorption in the multi-quantum well, and $f_s = \gamma_s/(\Omega_R^2/\gamma_2)$ is a parameter describing residual absorption in MQW at high pumping intensities, such as absorption in the unbound hot electron gas, normalized to the effective absorption rate in MQW (see Supplement 1 for a detailed derivation).

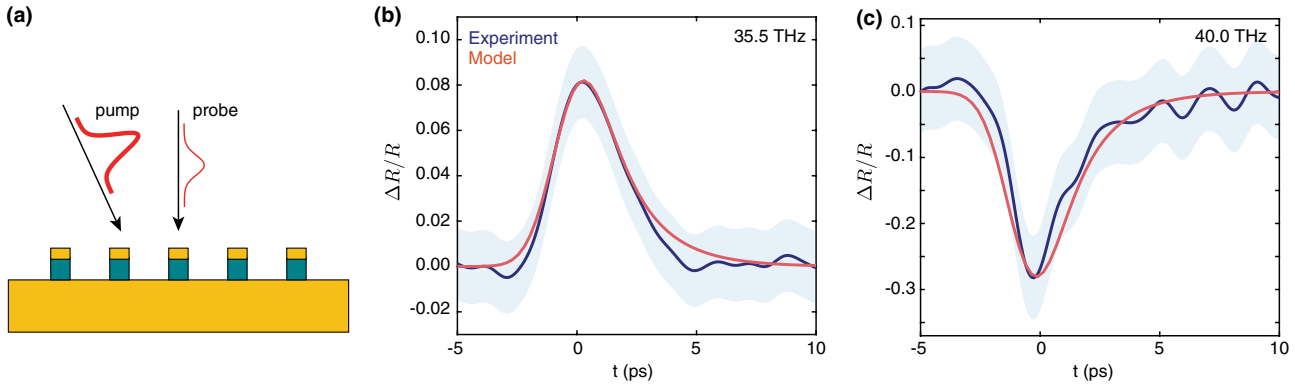

Fig. 4. Transient all-optical control of metasurface reflection. (a) Schematic showing the all-optical control experiment. A pump pulse excites the metasurface at an oblique angle, while a weaker pulse probes the metasurface response under normal incidence with time difference t. (b) A degenerate pump-probe measurement at 35.5 THz, demonstrating how the reflectivity can be increased all-optically at ultrafast timescales. The measurements are in excellent agreement with theoretical predictions based on Eq. (2), shown in red (with a peak intensity of 12.5 kW/cm^2). Shaded areas show measurement uncertainty. (c) A similar measurement performed at a different frequency to demonstrate optical limiting (40 THz), showing that reflectivity can also be all-optically reduced, highlighting the versatility of the metasurface operation. The red line again shows theoretical predictions based on Eq. (2), now for a peak intensity of 30 kW/cm^2.

An example of optical limiting is shown in the top of Fig. 5(a), where at high intensity the metasurface is critically coupled, while at low intensity, mode splitting results in low absorption at the same frequency. This example corresponds to $\eta = 0.031$ and $f_s = 0.08$, resulting in $|\Delta A| = 0.65$. The absorption contrast for other parameter combinations is shown in the bottom part of Fig. 5(a), where this particular example is highlighted with a circle. The contour plot highlights that optimal performance is simply governed by the two parameters η and f_s, one corresponding to photonic engineering, the other to material engineering. The lower the two can be made, the larger the reflection contrast that can be achieved. Improved performance in our metasurfaces can be achieved using dielectric resonators rather than metallic, to minimize η by avoiding metal absorption, and improving the MQW system to minimize the level of absorption in the saturation regime, for example by reducing the decoherence rate γ_2.

For the opposite process, the design of optimal metasurfaces with saturable absorption functionality, there are two approaches available. We can still work at the bare resonance frequencies but start with a critically coupled system at low intensity that becomes undercoupled at high intensity. In this case, the absorption contrast is exactly the same as derived for optical limiting in Eq. (3). The other approach to metasurface saturable absorption is shown in Fig. 5(b), where the frequency is aligned with a critically coupled normal mode at low intensity. In this case, the absorption contrast depends on three variables (γ_s/Ω_R, γ_a/Ω_R, and γ_2/Ω_R), and the final expression for the absorption contrast is more complicated (see Supplement 1 for details). We will therefore just highlight different regimes: one with very small $\gamma_2/\Omega_R = 0.1$ [Fig. 5(b)] and one with modest $\gamma_2/\Omega_R = 0.75$ [Fig. 5(c)] MQW dephasing rates, the latter example being more representative of the present experiment. We again find the largest contrast for small γ_a and γ_s, but we also see that a low γ_2/Ω_R clearly makes the system more forgiving, again making the case for further engineering of the MQW materials to reduce the decoherence rate. Note that these results are derived assuming that the rotating wave approximation is valid, which implies that when $\Omega_R/\omega_q \gtrapprox 0.1$, the applicability of these limits should be verified using numerical simulations (see Supplement 1). Deep in the ultrastrong coupling regime, these limits may differ significantly.

In the experiment presented in this manuscript, we find that our designs yield $f_s \approx 0.32$ and $\eta \approx 0.09$, respectively, predicting a maximum optical limiting contrast $|\Delta A| = 0.2$. Interestingly, this is below the change in absorption that we actually observe ($|\Delta A| \approx 0.3$), which is a consequence of the finite reflection at high intensity: the polaritonic metasurface is underdamped (γ_2 is too small) to be critically coupled at high intensity. Increasing γ_2 would also result in higher absorption at low intensity, reducing the overall absorption contrast. Furthermore, our theory demonstrates that in our metasurface residual absorption in the MQW is the limiting factor to achieve larger contrast: by reducing γ_s in the MQW, we may expect better optical limiting, especially when combined with lower loss metals or dielectric designs and narrower MQW linewidths. We are currently exploring these venues.

6. NONLINEAR PHASE-GRADIENT METASURFACE

Highly nonlinear optical response in deeply subwavelength nanoresonators composing our metasurface can enable all-optical manipulation of the reflected beam wave front using relatively low pumping intensities. This capability is demonstrated in Fig. 6, where we show the simulation results of power dependent beam deflection. An imprinted phase profile on the reflected beam is used to deflect the incident beam at arbitrary angles [56]. Due to the nonlinear response, the incident beam at low powers is reflected specularly [Fig. 6(a)], while at high power it is deflected into a single diffracted order at 30° [Fig. 6(b)].

The nonlinear metasurface consists of the same antennas studied in the previous sections. We now form a supercell consisting of six antennas, the length of each adjusted to have the correct phase in reflection following the design procedure outlined in Ref. [57]. The unit cell is now 2.5 by 15 μm, and the six antennas have lengths 740, 1195, 1242, 1270, 1302, and 1379 nm, respectively, so that the local reflection phase of the antennas themselves is 120, 60, 0, −60, −120, and −180, respectively. In the low power regime, due to polaritonic splitting, at 42 THz the antenna is barely excited, and we obtain specular reflection (because no

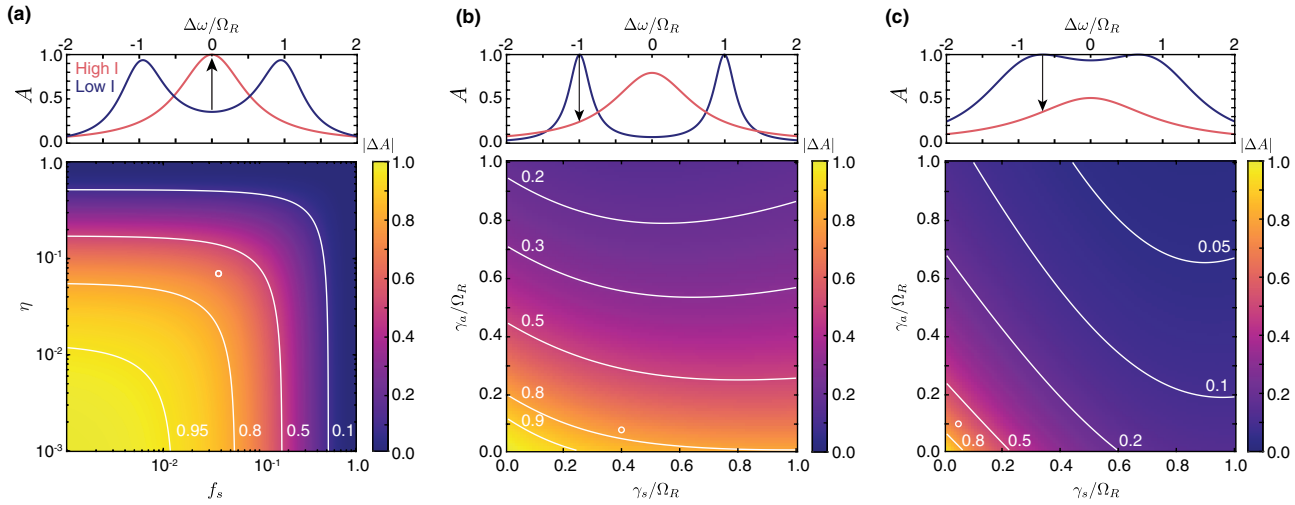

Fig. 5. Limits to metasurface absorption contrast. (a) Saturable and reverse saturable absorption when aligned with the bare resonance frequencies. The top part shows an example of reverse saturable absorption with critical coupling at high intensity. The bottom part shows the absorption contrast achieved for combinations of η and f_s, where the circle corresponds to the parameters in the top subplot. (b) Similar to (a), but now for saturable absorption when aligned with a critically coupled normal mode at low intensity, when $\gamma_2/\Omega_R = 0.1$. (c) Saturable absorption when aligned with a critically coupled normal mode at low intensity, when $\gamma_2/\Omega_R = 0.75$.

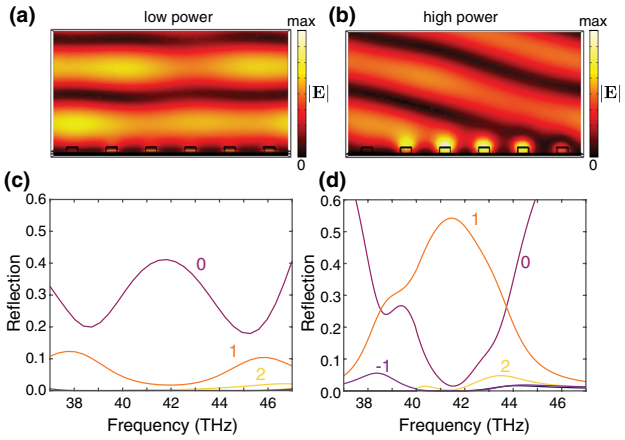

Fig. 6. Power-dependent beam deflection. (a) The absolute value of the electric field of the outgoing radiation near the nonlinear polaritonic metasurface excited at normal incidence at 42 THz. Based on the interference pattern, the response is dominated by specular reflection. (b) At high incident intensity, instead, the incident wave is reflected into the first diffracted order (30°). (c) The reflected power into each diffracted order (−1 and −2 not labeled because they are negligible) at low pumping intensity. At 42 THz reflection is largely specular due to polaritonic splitting. (d) At high power, the polaritonic splitting vanishes as demonstrated earlier in this work. Now, rather than achieving critical coupling and limiting functionality, the incident wave is reflected into the first diffracted order.

phase profile is imprinted). This can be seen in Fig. 6(c), where the reflection into each diffracted order is shown. At high intensity, however, the polaritonic splitting vanishes, and the beam is largely reflected into the first diffracted order, as shown in Fig. 6(d). These results demonstrate that, besides optical limiting (Fig. 4) and all-optical reflectivity control (Fig. 5) discussed in detail earlier, the highly nonlinear meta-atoms demonstrated in this work enable other, more complicated functionalities. These more advanced functionalities will be the subject of further theoretical and experimental analysis in a future study.

7. CONCLUSIONS

In summary, we have experimentally demonstrated ultra-fast mid-infrared nonlinear polaritonic metasurfaces that display strong optical limiting and power saturation in reflection. The ultrafast switching of the metasurface reflectivity is based on the optical control of the coupling constant between a MQW intersubband transition and an optical mode in a patch antenna. To the best of our knowledge, the presented metasurface has the largest ultra-fast third-order nonlinear absorption coefficient reported in the mid- or near-infrared range, enabling dramatic spectral changes at low input powers with large speed. We discussed what limits the absorption contrast in these structures, and determined the relevant design parameters, in terms of material and photonic engineering, required to achieve optimal performance for power limiting and saturable absorption. We foresee applications of these ultrathin metasurfaces for optical limiters, all-optical low-power switches, and saturable absorbers. By tailoring the meta-atoms across different unit cells, incorporating, e.g., a geometric phase, these metasurfaces may provide advanced linear and intensity-dependent nonlinear responses that may be used for optical control of the intensity, polarization state, and wavefront of the reflected beam.

APPENDIX A: METHODS

Sample Fabrication: Fabrication of the intersubband polaritonic metasurface described in this work began with growth of the MQW structure by molecular beam epitaxy on an InP substrate. The wafer was first metallized via e-beam evaporation with Ti, Pt, and Au layers of 10, 20, and 200 nm, respectively, and thermo-compressively bonded to a foreign InP substrate with identical metal layers to form a metal backplane. The original substrate was then removed via mechanical polishing and selective wet chemical etching. 10 nm of Ti and 100 nm of Au were evaporated to form the top metal, followed by a 300-nm-thick SiNx hard mask layer. The dipole resonators were then defined via electron-beam lithography and successive dry etching steps, and finally, the hard mask

was removed. To account for the uncertainty of material parameters such as metal loss and experimental radiative loss of the dipole array, we fabricated dipole antennas with varying lengths and unit cell sizes.

Intensity-Dependent Response: The mid-IR output of a picosecond optical parametric oscillator (OPO)/difference frequency generation (DFG) system (Carmina, APE) with ∼1.6 ps intensity FWHM pulses at a 40 MHz repetition rate was focused onto the metasurface under study through a mid-IR transmissive BaF_2 lens. We control the intensity of the pump source by using a wire-grid linear polarizer pair, where the first polarizer is rotated to attenuate the polarized output of the OPG/OPA throughout the intensity-dependent measurements, and the second polarizer is rotated and held constant to ensure light is polarized along the IPM dipole axis. The incident and reflected power are measured simultaneously by two Mercury–Cadmium–Telluride (MCT) photodetectors placed on either side of a wedge ZnSe beam-splitter in front of the BaF_2 lens. We simultaneously measure a fraction of the incident and reflected beams using two separate detectors to account for any variations in laser power, and normalize results from our IPMs to an Au mirror reference, which does not produce an intensity-dependent optical response.

Degenerate Pump-Probe Experiment: The mid-IR output of a ps-OPO/DFG system is split into strong pump and weak probe beam paths. The pump beam is focused onto the metasurface under an angle, while the probe is directed toward a retroreflector mounted on a delay stage, and then focused at normal incidence onto the metasurface at the same spatial location. The incident and reflected powers of the probe path are simultaneously monitored by way of two MCT photodetectors placed on either side of a wedge ZnSe beam-splitter in front of the sample, and time-dependent reflectivity is retrieved by monitoring the reflectivity recovered from the probe beam as a function of the pump-probe delay.

Funding. Defense Advanced Research Projects Agency; Air Force Office of Scientific Research; Office of Naval Research; U.S. Department of Defense; Nederlandse Organisatie voor Wetenschappelijk Onderzoek (019.172EN.019); U.S. Department of Energy; National Nuclear Security Administration (DE-NA0003525).

Acknowledgment. IB and JK acknowledge support by the U.S. Department of Energy, Office of Basic Energy Sciences, Division of Materials Sciences and Engineering. This paper describes objective technical results and analysis. Any subjective views or opinions that might be expressed in the paper do not necessarily represent the views of the U.S. Department of Energy or the United States Government. Sample processing was done at the University of Texas at Austin Microelectronics Research Center, which is a member of the National Science Foundation National Nanotechnology Coordinated Infrastructure (NSF NNCI).

Disclosures. The authors declare no conflicts of interest.

Data Availability. Data underlying the results presented in this paper are not publicly available at this time but may be obtained from the authors upon reasonable request.

Supplemental document. See Supplement 1 for supporting content.

†These authors contributed equally to this paper.

REFERENCES

1. M. Kauranen and A. V. Zayats, "Nonlinear plasmonics," Nat. Photonics **6**, 737–748 (2012).
2. H. Baida, D. Mongin, D. Christofilos, G. Bachelier, A. Crut, P. Maioli, N. Del Fatti, and F. Vallée, "Ultrafast nonlinear optical response of a single gold nanorod near its surface plasmon resonance," Phys. Rev. Lett. **107**, 057402 (2011).
3. M. Ren, B. Jia, J.-Y. Ou, E. Plum, J. Zhang, K. F. MacDonald, A. E. Nikolaenko, J. Xu, M. Gu, and N. I. Zheludev, "Nanostructured plasmonic medium for terahertz bandwidth all-optical switching," Adv. Mater. **23**, 5540–5544 (2011).
4. Y. Yang, W. Wang, A. Boulesbaa, I. I. Kravchenko, D. P. Briggs, A. Puretzky, D. Geohegan, and J. Valentine, "Nonlinear Fano-resonant dielectric metasurfaces," Nano Lett. **15**, 7388–7393 (2015).
5. M. R. Shcherbakov, P. P. Vabishchevich, A. S. Shorokhov, K. E. Chong, D.-Y. Choi, I. Staude, A. E. Miroshnichenko, D. N. Neshev, A. A. Fedyanin, and Y. S. Kivshar, "Ultrafast all-optical switching with magnetic resonances in nonlinear dielectric nanostructures," Nano Lett. **15**, 6985–6990 (2015).
6. S. Liu, M. B. Sinclair, S. Saravi, G. A. Keeler, Y. Yang, J. Reno, G. M. Peake, F. Setzpfandt, I. Staude, T. Pertsch, and I. Brener, "Resonantly enhanced second-harmonic generation using III–V semiconductor all-dielectric metasurfaces," Nano Lett. **16**, 5426–5432 (2016).
7. V. V. Zubyuk, P. P. Vabishchevich, M. R. Shcherbakov, A. S. Shorokhov, A. N. Fedotova, S. Liu, G. Keeler, T. V. Dolgova, I. Staude, I. Brener, and A. A. Fedyanin, "Low-power absorption saturation in semiconductor metasurfaces," ACS Photon. **6**, 2797–2806 (2019).
8. L. Caspani, R. P. M. Kaipurath, M. Clerici, M. Ferrera, T. Roger, J. Kim, N. Kinsey, M. Pietrzyk, A. Di Falco, V. M. Shalaev, A. Boltasseva, and D. Faccio, "Enhanced nonlinear refractive index in ε-near-zero materials," Phys. Rev. Lett. **116**, 233901 (2016).
9. M. Z. Alam, S. A. Schulz, J. Upham, I. De Leon, and R. W. Boyd, "Large optical nonlinearity of nanoantennas coupled to an epsilon-near-zero material," Nat. Photonics **12**, 79–83 (2018).
10. M. Z. Alam, I. De Leon, and R. W. Boyd, "Large optical nonlinearity of indium tin oxide in its epsilon-near-zero region," Science **352**, 795–797 (2016).
11. N. Kinsey and J. Khurgin, "Nonlinear epsilon-near-zero materials explained: opinion," Opt. Mater. Express **9**, 2793–2796 (2019).
12. Y. Yang, K. Kelley, E. Sachet, S. Campione, T. S. Luk, J. P. Maria, M. B. Sinclair, and I. Brener, "Femtosecond optical polarization switching using a cadmium oxide-based perfect absorber," Nat. Photonics **11**, 390–395 (2017).
13. Y. Yang, J. Lu, A. Manjavacas, T. S. Luk, H. Liu, K. Kelley, J.-P. Maria, E. L. Runnerstrom, M. B. Sinclair, S. Ghimire, and I. Brener, "High-harmonic generation from an epsilon-near-zero material," Nat. Phys. **15**, 1022–1026 (2019).
14. P. Vasa, R. Pomraenke, G. Cirmi, E. De Re, W. Wang, S. Schwieger, D. Leipold, E. Runge, G. Cerullo, and C. Lienau, "Ultrafast manipulation of strong coupling in metal−molecular aggregate hybrid nanostructures," ACS Nano **4**, 7559–7565 (2010).
15. P. Vasa, W. Wang, R. Pomraenke, M. Lammers, M. Maiuri, C. Manzoni, G. Cerullo, and C. Lienau, "Real-time observation of ultrafast Rabi oscillations between excitons and plasmons in metal nanostructures with J-aggregates," Nat. Photonics **7**, 128–132 (2013).
16. N. T. Fofang, N. K. Grady, Z. Fan, A. O. Govorov, and N. J. Halas, "Plexciton dynamics: exciton−plasmon coupling in a J-aggregate−Au nanoshell complex provides a mechanism for nonlinearity," Nano Lett. **11**, 1556–1560 (2011).
17. A. Manjavacas, F. J. García de Abajo, and P. Nordlander, "Quantum plexcitonics: strongly interacting plasmons and excitons," Nano Lett. **11**, 2318–2323 (2011).
18. S. R. K. Rodriguez, J. Feist, M. A. Verschuuren, F. J. Garcia Vidal, and J. Gómez Rivas, "Thermalization and cooling of plasmon-exciton polaritons: towards quantum condensation," Phys. Rev. Lett. **111**, 166802 (2013).
19. J. Lee, M. Tymchenko, C. Argyropoulos, P.-Y. Chen, F. Lu, F. Demmerle, G. Boehm, M.-C. Amann, A. Alù, and M. A. Belkin, "Giant nonlinear response from plasmonic metasurfaces coupled to intersubband transitions," Nature **511**, 65–69 (2014).
20. J. Lee, N. Nookala, J. S. Gomez-Diaz, M. Tymchenko, F. Demmerle, G. Boehm, M. Amann, A. Alù, and M. A. Belkin, "Ultrathin second-harmonic metasurfaces with record-high nonlinear optical response," Adv. Opt. Mater. **4**, 664–670 (2016).
21. J. Khurgin, "Second-order nonlinear effects in asymmetric quantum-well structures," Phys. Rev. B **38**, 4056–4066 (1988).
22. C. Sirtori, F. Capasso, D. L. Sivco, S. N. G. Chu, and A. Y. Cho, "Observation of large second order susceptibility via intersubband

transitions at λ∼10 μm in asymmetric coupled AlInAs/GaInAs quantum wells," Appl. Phys. Lett. **59**, 2302–2304 (1991).
23. F. Capasso, C. Sirtori, and A. Y. Cho, "Coupled quantum well semiconductors with giant electric field tunable nonlinear optical properties in the infrared," IEEE J. Quantum Electron. **30**, 1313–1326 (1994).
24. E. Rosencher, A. Fiore, B. Vinter, V. Berger, P. Bois, and J. Nagle, "Quantum engineering of optical nonlinearities," Science **271**, 168–173 (1996).
25. M. Tymchenko, J. S. Gomez-Diaz, J. Lee, N. Nookala, M. A. Belkin, and A. Alù, "Gradient nonlinear Pancharatnam-Berry metasurfaces," Phys. Rev. Lett. **115**, 207403 (2015).
26. N. Nookala, J. Lee, M. Tymchenko, J. Sebastian Gomez-Diaz, F. Demmerle, G. Boehm, K. Lai, G. Shvets, M.-C. Amann, A. Alu, and M. Belkin, "Ultrathin gradient nonlinear metasurface with a giant nonlinear response," Optica **3**, 283–288 (2016).
27. O. Wolf, A. A. Allerman, X. Ma, J. R. Wendt, A. Y. Song, E. A. Shaner, and I. Brener, "Enhanced optical nonlinearities in the near-infrared using III-nitride heterostructures coupled to metamaterials," Appl. Phys. Lett. **107**, 151108 (2015).
28. Y. Liu, J. Lee, S. March, N. Nookala, D. Palaferri, J. F. Klem, S. R. Bank, I. Brener, and M. A. Belkin, "Difference-frequency generation in polaritonic intersubband nonlinear metasurfaces," Adv. Opt. Mater. **6**, 1800681 (2018).
29. J. S. Gomez-Diaz, M. Tymchenko, J. Lee, M. A. Belkin, and A. Alù, "Nonlinear processes in multi-quantum-well plasmonic metasurfaces: electromagnetic response, saturation effects, limits, and potentials," Phys. Rev. B **92**, 125429 (2015).
30. S. Zanotto, R. Degl'Innocenti, J.-H. Xu, L. Sorba, A. Tredicucci, and G. Biasiol, "Ultrafast optical bleaching of intersubband cavity polaritons," Phys. Rev. B **86**, 201302 (2012).
31. R. Butté, G. Delalleau, A. I. Tartakovskii, M. S. Skolnick, V. N. Astratov, J. J. Baumberg, G. Malpuech, A. Di Carlo, A. V. Kavokin, and J. S. Roberts, "Transition from strong to weak coupling and the onset of lasing in semiconductor microcavities," Phys. Rev. B **65**, 205310 (2002).
32. A. Benz, S. Campione, S. Liu, I. Montaño, J. F. Klem, A. Allerman, J. R. Wendt, M. B. Sinclair, F. Capolino, and I. Brener, "Strong coupling in the sub-wavelength limit using metamaterial nanocavities," Nat. Commun. **4**, 2882 (2013).
33. G. Khitrova and H. M. Gibbs, "Nonlinear optics of normal-mode-coupling semiconductor microcavities," Rev. Mod. Phys. **71**, 1591–1639 (1999).
34. S. Zanotto, F. Bianco, L. Sorba, G. Biasiol, and A. Tredicucci, "Saturation and bistability of defect-mode intersubband polaritons," Phys. Rev. B **91**, 085308 (2015).
35. Y. Todorov, A. M. Andrews, R. Colombelli, S. De Liberato, C. Ciuti, P. Klang, G. Strasser, and C. Sirtori, "Ultrastrong light-matter coupling regime with polariton dots," Phys. Rev. Lett. **105**, 196402 (2010).
36. G. Günter, A. A. Anappara, J. Hees, A. Sell, G. Biasiol, L. Sorba, S. De Liberato, C. Ciuti, A. Tredicucci, A. Leitenstorfer, and R. Huber, "Sub-cycle switch-on of ultrastrong light-matter interaction," Nature **458**, 178–181 (2009).
37. P. Jouy, A. Vasanelli, Y. Todorov, A. Delteil, G. Biasiol, L. Sorba, and C. Sirtori, "Transition from strong to ultrastrong coupling regime in mid-infrared metal-dielectric-metal cavities," Appl. Phys. Lett. **98**, 10–13 (2011).
38. Y. Todorov, A. M. Andrews, I. Sagnes, R. Colombelli, P. Klang, G. Strasser, and C. Sirtori, "Strong light-matter coupling in subwavelength metal-dielectric microcavities at terahertz frequencies," Phys. Rev. Lett. **102**, 186402 (2009).
39. A. Frisk Kockum, A. Miranowicz, S. De Liberato, S. Savasta, and F. Nori, "Ultrastrong coupling between light and matter," Nat. Rev. Phys. **1**, 19–40 (2019).
40. D. Palaferri, Y. Todorov, A. Mottaghizadeh, G. Frucci, G. Biasiol, and C. Sirtori, "Ultra-subwavelength resonators for high temperature high performance quantum detectors," New J. Phys. **18**, 113016 (2016).
41. M. Diem, T. Koschny, and C. M. Soukoulis, "Wide-angle perfect absorber/thermal emitter in the terahertz regime," Phys. Rev. B **79**, 033101 (2009).
42. J. Le Perchec, Y. Desieres, N. Rochat, and R. Espiau De Lamaestre, "Subwavelength optical absorber with an integrated photon sorter," Appl. Phys. Lett. **100**, 113305 (2012).
43. Y. Ra'di, C. R. Simovski, S. A. Tretyakov, Y. Ra, C. R. Simovski, and S. A. Tretyakov, "Thin perfect absorbers for electromagnetic waves: theory, design, and realizations," Phys. Rev. Appl. **3**, 037001 (2015).
44. S. A. Mann and E. C. Garnett, "Resonant nanophotonic spectrum splitting for ultrathin multijunction solar cells," ACS Photon. **2**, 816–821 (2015).
45. P. T. Bowen, A. Baron, and D. R. Smith, "Theory of patch-antenna metamaterial perfect absorbers," Phys. Rev. A **93**, 063849 (2016).
46. D. Dini, R. Köhler, A. Tredicucci, G. Biasiol, and L. Sorba, "Microcavity polariton splitting of intersubband transitions," Phys. Rev. Lett. **90**, 116401 (2003).
47. F. Arecchi and R. Bonifacio, "Theory of optical maser amplifiers," IEEE J. Quantum Electron. **1**, 169–178 (1965).
48. S. L. McCall and E. L. Hahn, "Self-induced transparency by pulsed coherent light," Phys. Rev. Lett. **18**, 908–911 (1967).
49. F. Bloch, "Nuclear induction," Phys. Rev. **70**, 460–474 (1946).
50. R. A. Shah, N. F. Scherer, M. Pelton, and S. K. Gray, "Ultrafast reversal of a Fano resonance in a plasmon-exciton system," Phys. Rev. B **88**, 075411 (2013).
51. H. A. Haus, *Waves and Fields in Optoelectronics* (Prentice-Hall, 1984).
52. J. L. Cheng, N. Vermeulen, and J. E. Sipe, "Third order optical nonlinearity of graphene," New J. Phys. **16**, 053014 (2014).
53. X. Liu, Q. Guo, and J. Qiu, "Emerging low-dimensional materials for nonlinear optics and ultrafast photonics," Adv. Mater. **29**, 1605886 (2017).
54. U. Keller, K. J. Weingarten, F. X. Kärtner, D. Kopf, B. Braun, I. D. Jung, R. Fluck, C. Hönninger, N. Matuschek, and J. Aus Der Au, "Semiconductor saturable absorber mirrors (SESAM's) for femtosecond to nanosecond pulse generation in solid-state lasers," IEEE J. Sel. Top. Quantum Electron. **2**, 435–451 (1996).
55. D. A. B. Miller, "Quantum well self-electro-optic effect devices," Opt. Quantum Electron. **22**, S61–S98 (1990).
56. N. Yu, P. Genevet, M. A. Kats, F. Aieta, J.-P. Tetienne, F. Capasso, and Z. Gaburro, "Light propagation with phase discontinuities: generalized laws of reflection and refraction," Science **334**, 333–337 (2011).
57. A. Mekawy, M. Khalifa, T. A. Ali, and A. H. Badawi, "Tuning optical properties of metasurface via piezoelectric effect," IET Optoelectron. **13**, 134–138 (2019).